Journal of Applied Mechanics and Technical Physics, Vol. 42, No. 2, pp. 363–370, 2001

APPLICATION OF WAVELET ANALYSIS TO IDENTIFICATION OF STRUCTURALLY INHOMOGENEOUS DEFORMABLE MATERIALS

V. V. Zverev,[1] A. G. Zalazinskii,[2]
V. I. Novozhonov,[3] and A. P. Polyakov[2]

UDC 517:621.777:669.2

A wavelet-based experimental technique for studying the structure of material surfaces is proposed. The basic theoretical concepts of the local-frequency and wavelet analyses are given. Examples of the wavelet analysis of model images are considered. The structure of briquettes obtained by compaction of titanium sponge is determined with the use of wavelet analysis.

It is of interest to study the dependence of the physicomechanical properties of strongly inhomogeneous deformable materials (composites, powdered materials, etc.) on their macro- and microstructures. In this connection, one needs information on the integral characteristics of the structure to be studied such as the spatial frequency of repetition of the elements (for example, grains, pores, or cracks), the statistical characteristic of their distribution, the presence of scale invariance, etc. [1]. Below, we consider the basic concepts of the technique developed by the authors to study experimentally the structure of a material with the use of the wavelet analysis, which was evolved intensely in the last decade of the 20th century [2–8]. In our opinion, this technique allows one to identify a deformable material, determine the periodicity of its micro- and macrostructures, and estimate the dimensions of representative elementary volumes for determination of the effective mechanical characteristics in solving problems of the mechanics of deformable structurally inhomogeneous materials.

The wavelet-based methods enable one to calculate the local and integral characteristics of images within the framework of a unified procedure of decompositon into wavelet spectra, determine the structure of a strongly inhomogeneous volume, and study its local scale (scale-invariance) properties, since the wavelet transform yields a two-dimensional scan of the one-dimensional signal to be investigated (the frequency and coordinates are considered as independent variables). As a result, it is possible to analyze the properties of the signal in the physical (space and time) and frequency spaces simultaneously [4]. The wavelet analysis can also be used to study both time sequences and spatial distributions [7].

The existing mathematical methods of analyzing the local-frequency distributions are closely related to the concepts of quantum mechanics which admit a quantum–classical correspondence. Indeed, in the quantum theory of Hamiltonian systems, in addition to the coordinate and momentum representations, the continuous (c-number) Weyl representation is widely used [9, 10], in which the statistical operator is replaced by the Wigner function [11, 12] defined in the c-number coordinate-momentum (phase) space; this function becomes a standard distribution function determined in statistical mechanics in the limiting case as $\hbar \to 0$. Since the coordinate-momentum representation is determined by the Fourier transform (decomposition of the functions into a continuous frequency spectrum), the mathematical apparatus of the Weyl representation can be extended to a broad range of problems of spectral analysis.

[1]Ural State Technical University, Ekaterinburg 620002. [2]Institute of Machine Science, Ural Division, Russian Academy of Sciences, Ekaterinburg 620219. [3]Institute of Metal Physics, Ural Division, Russian Academy of Sciences, Ekaterinburg 620219. Translated from Prikladnaya Mekhanika i Tekhnicheskaya Fizika, Vol. 42, No. 2, pp. 199–207, March–April, 2001. Original article submitted August 23, 2000.

0021-8944/01/4202-0363 $25.00

We give some relations used to replace the statistical operator $\hat{\rho} = \sum\limits_{ij} w_{ij}|i\rangle\langle j|$ $\Big(\mathrm{sp}\,\hat{\rho} = \sum\limits_{i} w_{ii} = 1\Big)$ by the Wigner function [11, 12] (the standard Dirac notation is used). Introducing the coordinate and momentum representations (one-dimensional model), we obtain

$$\rho_x(x, x') \equiv \langle x|\hat{\rho}|x'\rangle = \sum_{ij} w_{ij}\varphi_i(x)\varphi_j^*(x'), \qquad \varphi_i(x) = \langle x|i\rangle,$$

$$\rho_p(p, p') \equiv \langle p|\hat{\rho}|p'\rangle = \sum_{ij} w_{ij}\varphi_i(p)\varphi_j^*(p') = \int\limits_{-\infty}^{\infty}\int\limits_{-\infty}^{\infty} \rho_x(x, x') \exp\Big[-\frac{i}{\hbar}\,(px - p'x')\Big]\,dx\,dx'.$$

The transformation from the matrix element of the statistical operator in the coordinate representation to the Wigner function and the inverse transformation to coordinate and momentum representations are performed according to the rules

$$f_w(p, x) = \int\limits_{-\infty}^{\infty} \rho_x\Big(x + \frac{1}{2}\,\eta, x - \frac{1}{2}\,\eta\Big) \exp\Big(-\frac{i}{\hbar}\,p\eta\Big)d\eta; \tag{1}$$

$$\rho_x(x, x') = (2\pi\hbar)^{-1} \int\limits_{-\infty}^{\infty} f_w\Big(p, \frac{1}{2}\,(x + x')\Big) \exp\Big[\frac{i}{\hbar}\,p(x - x')\Big]dp; \tag{2}$$

$$\rho_p(p, p') = \int\limits_{-\infty}^{\infty} f_w\Big(\frac{1}{2}\,(p + p'), x\Big) \exp\Big[-\frac{i}{\hbar}\,x(p - p')\Big]dx. \tag{3}$$

The properties of the Wigner and usual distribution functions are similar in many respects. Indeed, the formulas for calculating the means of arbitrary functions that depend only on the coordinate or momentum have the same form as those in the classical theory:

$$\mathrm{sp}\,(\hat{\rho}g(\hat{x})) = \sum_{ij} w_{ij}\langle i|g(\hat{x})|j\rangle = \int\limits_{-\infty}^{\infty}\int\limits_{-\infty}^{\infty} f_w(x, p)g(x)\,\frac{dp\,dx}{2\pi\hbar},$$

$$\mathrm{sp}\,(\hat{\rho}g(\hat{p})) = \sum_{ij} w_{ij}\langle i|g(\hat{p})|j\rangle = \int\limits_{-\infty}^{\infty}\int\limits_{-\infty}^{\infty} f_w(x, p)g(p)\,\frac{dp\,dx}{2\pi\hbar}.$$

In the case where the statistical operator describes a "pure" quantum-mechanical state, formulas (1)–(3) become

$$\rho(x, x') = \varphi(x)\varphi^*(x'), \quad f_w(p, x) = \int\limits_{-\infty}^{\infty} \varphi\Big(x + \frac{1}{2}\,\eta\Big)\varphi^*\Big(x - \frac{1}{2}\,\eta\Big) \exp\Big(-\frac{i}{\hbar}\,p\eta\Big)d\eta. \tag{4}$$

The similar structure of the right sides in expressions (2) and (3) reflects the fact that the Weyl representation is in an intermediate position between the coordinate and momentum representations. If the momentum and coordinate values are completely uncertain in the coordinate and momentum representations, respectively, the Weyl representation ensures a "compromise" and minimizes the uncertainty of each quantity to an extent admitted by the uncertainty relation. If the spectral analysis of a sequence of data is performed by the Fourier transform, transformations (1)–(3) allows one to consider the local-frequency characteristics of such sequences (in particular, the nonstationary signals or spatial distributions obtained experimentally).

Following Walker [6] and Torresani [8], we consider the possible generalizations of the Weyl representation to the general problems of spectral analysis. For certainty, we assume that the initial functions depend on time. Let the integral Fourier transform have the form

$$\hat{f}(\omega) = \int\limits_{-\infty}^{\infty} f(t) \exp(-i\omega t)\, dt, \qquad f(t) = \frac{1}{2\pi} \int\limits_{-\infty}^{\infty} \hat{f}(\omega) \exp(i\omega t)\, d\omega.$$

We assume that $f(t)$ and $g(t)$ are certain complex signals. By analogy with the Wigner function (4), we introduce the functions

$$R_{f,g}(\tau, \xi) = \int\limits_{-\infty}^{\infty} f\Big(t + \frac{1}{2}\tau\Big) g^*\Big(t - \frac{1}{2}\tau\Big) \exp(-i\xi t)\, dt; \tag{5}$$

$$E_{f,g}(b, \omega) = \int\limits_{-\infty}^{\infty} f\Big(b + \frac{1}{2}\tau\Big) g^*\Big(b - \frac{1}{2}\tau\Big) \exp(-i\omega\tau)\, d\tau. \tag{6}$$

With allowance for the replacement $b + \tau/2 = q$, we rewrite the last expression in the form

$$E_{f,g}(b, \omega) = 2 \int\limits_{-\infty}^{\infty} f(q) g^*(2b - q) \exp[-i\omega(q - b)]\, dq. \tag{7}$$

Functions (5) and (6), which are called, in [18], the uncertainty cross function and the Wigner–Wille cross function, respectively, are related through the symplectic Fourier transform:

$$R_{f,g}(\tau, \xi) = \frac{1}{2\pi} \int\limits_{-\infty}^{\infty} \int\limits_{-\infty}^{\infty} E_{f,g}(b, \omega) \exp[-i(\xi b - \omega\tau)]\, db\, d\omega,$$

$$E_{f,g}(b, \omega) = \frac{1}{2\pi} \int\limits_{-\infty}^{\infty} \int\limits_{-\infty}^{\infty} R_{f,g}(\tau, \xi) \exp[i(\xi b - \omega\tau)]\, d\tau\, d\xi.$$

To illustrate the application of the time–frequency analysis by means of the function (6), we consider the problem of processing a radar signal in an idealized formulation. Let a "radar" send a short radio pulse $f(t)$ with a delta-shaped envelope and high-frequency filling with a frequency Ω. The reflected pulse $g(t)$ has a time lag, and the filling frequency changes by ω_0 (due to the Doppler effect). Assuming that the reflected signal is represented in the form $g(t) = A \exp[i\omega_0(t - t_0)] f(t - t_0)$ (for simplicity, the shape of the envelope is assumed to be the same), we calculate approximately the magnitude of the Wigner–Wille function

$$|E_{f,g}(b, \omega)| \approx k|A|\, |\hat{f}(\Omega)|^2 \delta(2\omega - 2\Omega - \omega_0) \delta(2b - t_0). \tag{8}$$

On the right side of expression (8), the delta-shaped functions are written in the form of delta functions and the constant k depends on the shape of the envelope. Function (8) has a narrow peak for $b \approx t_0/2$ and $\omega \approx \omega_0/2$. Thus, comparing the initial and returned signals, we find the time lag and the frequency shift, i.e., we perform the time–frequency analysis.

We now consider formula (7). When the function $g(t)$ is fixed, expression (7) is a certain integral transform on the set of functions $f(t)$. We define a transformation called the continuous Gabor or "window" Fourier transform [8]:

$$G_f(b, \omega) = \langle f, g_{b,\omega} \rangle \equiv \int\limits_{-\infty}^{\infty} f(t) g^*_{b,\omega}(t)\, dt.$$

Here $g_{b,\omega}(t) = \exp[i\omega(t - b)] g(t - b)$ is the Gabor function. The function $g_{b,\omega}$ is the product of the oscillating exponent function and the "window" function $g(t)$; as a "window" function, one can use, for example, the Gaussian function or a function of the rectangular-pulse type. The inverse Gabor transform is given by

$$f(t) = (2\pi \|g\|^2)^{-1} \int\limits_{-\infty}^{\infty} \int\limits_{-\infty}^{\infty} G_f(b, \omega) g_{b,\omega}(t)\, db\, d\omega, \quad \|g\|^2 = \int\limits_{-\infty}^{\infty} db |g(b)|^2.$$

We show that the conversion formula of the Gabor transform allows one to take into account the slow variation in the filling frequency in the range of change of the envelope pulse. Let $f(t) = A(t)\exp[i\varphi(t)]$, where $\varphi(t) = \omega(t)t$ and $t\omega'(t) \ll \omega(t)$ for all values of t at which the function of the envelope shape $A(t)$ differs significantly from zero (i.e., the frequency varies insignificantly within the boundaries of the window). In this case, we have $\varphi'(t) \approx \omega(t)$. Assuming that $\varphi(t) \approx \varphi(b) + \varphi'(b)(t-b)$, after certain manipulations we obtain

$$|G_f(b,\omega)| = \langle f, g_{b,\omega}\rangle \approx |A(b)|\,|\hat{g}(\varphi'(b)-\omega)|. \tag{9}$$

It follows from expression (9) that one can find (with a certain error) the envelope shape $|A(b)|$ by varying b; fixing b and varying ω, one can also determine the local value of the frequency by localizing the maximum of the Fourier transform of the "window" function: $\omega_{\max} \approx \varphi'(b) \approx \omega(b)$.

The "window" Fourier transform is an effective means of processing complex signals. One of its shortcomings is that the function image depends on many variables. Even in the one-dimensional case, there are three variables: the position of the middle of the window, its width, and the frequency of oscillations filling the window; moreover, the last two variables cannot be chosen independently. The above-described approach can be simplified if one fixes the number of oscillations that fill the window, for example, by keeping a constant ratio of the window width to the period of oscillations. In this case, the number of variables reduces to two, and the necessary variation in the window parameters is performed by scaling the window together with its "filling." This idea forms the basis of a new modification of time–frequency analysis which is called the multiple-resolvent (wavelet) analysis.

We consider the wavelet function $\psi(t)$. Its graph must look as a window filled with oscillations. We construct the basis by performing the continuous scale transformations and translations of this function:

$$\psi_{a,b}(t) = \frac{1}{\sqrt{|a|}}\,\psi\Big(\frac{t-b}{a}\Big), \qquad a \in \mathbb{R}, \qquad b \in \mathbb{R}.$$

We determine the continuous wavelet transform of an arbitrary function $f(t)$:

$$W_f(a,b) = \langle f, \psi_{a,b}\rangle \equiv \int\limits_{-\infty}^{\infty} f(t)\psi^*_{a,b}(t)\,dt. \tag{10}$$

The Fourier transform of the basis function is related to the Fourier transform of the wavelet by the relation $\hat{\psi}_{a,b}(\omega) = (a/\sqrt{|a|})\exp(-i\omega b)\hat{\psi}(a\omega)$. Using the Parseval equality $2\pi\langle f, g\rangle = \langle \hat{f}, \hat{g}\rangle$, one can establish the formulas for the inverse wavelet transform

$$f(x) = \frac{1}{c_\psi}\int\limits_{-\infty}^{\infty}\int\limits_{-\infty}^{\infty} W_f(a,b)\psi_{a,b}(x)\,\frac{da\,db}{a|a|}, \qquad C_\psi = \int\limits_{-\infty}^{\infty}\frac{d\xi}{\xi}\,|\hat{\psi}(\xi)|^2.$$

We show that the wavelet transform allows one to take into account slow variation of the filling frequency within the confines of the radio-pulse envelope. Let $f(t) = A(t)\exp[i\varphi(t)]$ and $\varphi(t) = \omega(t)t$ and $t\omega'(t) \ll \omega(t)$ for all the values of t within the confines of the pulse envelope. Then, $|W_f(a,b)| \approx \sqrt{|a|}\,|A(b)|\,|\hat{\psi}(a\varphi'(b))|$. We assume that the Fourier transform of the wavelet function $\hat{\psi}(\omega)$ reaches an extremum at the point $\omega_0 \neq 0$ on the frequency axis. Determining the extremum as a function of a (for b fixed), we find $\varphi'(b) \approx \omega(b)$ by solving the equation $a\varphi'(b) \approx \omega_0$. In logarithmic form, this equation becomes $\log_2 a \approx \log_2\omega_0 - \log_2\varphi'(b)$. Thus, if the frequency of the signal decreases by twofold, the extremum shifts along the $\log_2 a$ axis by unity.

It is convenient to choose the real wavelet functions in the form of derivatives of the Gaussian function:

$$\psi(t) = (-1)^{m+1}\frac{d^m}{dt^m}\exp\Big(-\frac{t^2}{2}\Big) \qquad (m \geqslant 1). \tag{11}$$

Morlet introduced another type of wavelet function [3]: $\psi(t) = \exp(i\omega_0 t)\exp(-t^2/2)$. The wavelet transform proposed by Morlet is similar to the window Fourier transform, since the wavelet function is a Gaussian window filled by sinusoidal oscillations. For $m = 2$, function (11) is used most frequently and referred to as the "Mexican hat" or "sombrero" wavelet. Another examples of the frequently used wavelet functions are given in [4].

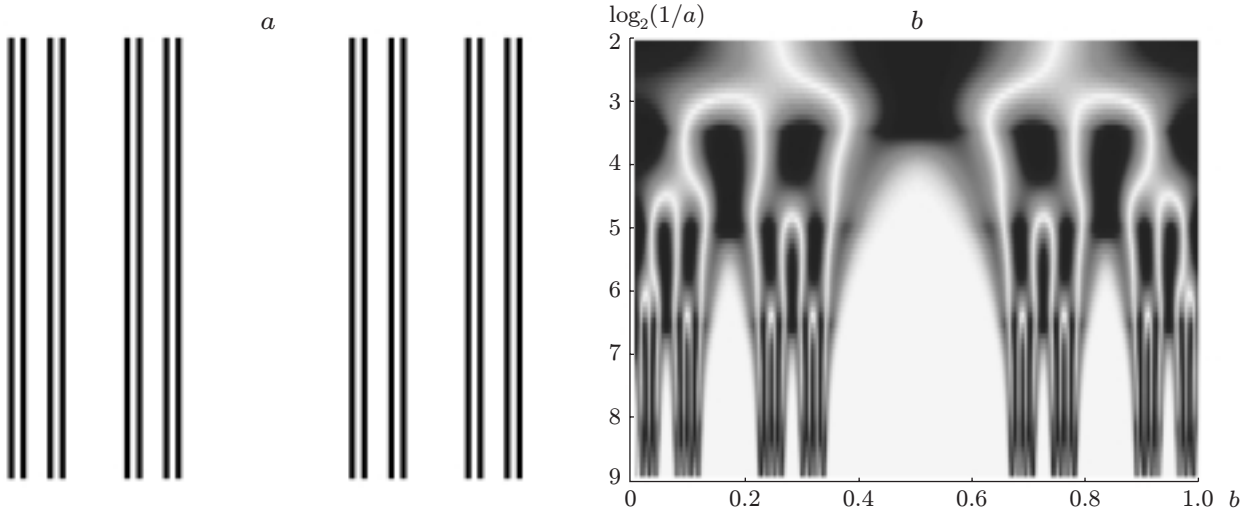

Fig. 1. Scale-invariant raster (a) and its waveletogram (b).

Let us apply the wavelet analysis to a series of artificially obtained images. We construct a raster with the scale invariance (self-similarity) in the form of a set of black bands (Fig. 1a) by means of the algorithm for constructing the Cantor set. We divide the black rectangle by segments parallel to the lateral sides into three equal parts and remove the central part. We repeat this procedure for each of the other parts, etc. As a function $f(t)$, we use the one-dimensional distribution obtained by scanning the raster along the horizontal line from $t = 0$ (the left boundary of the image) to $t = 1$ (the right boundary of the image). The value of the function is proportional to the degree of blackening of the image. In the waveletogram shown in Fig. 1b ("sombrero" wavelet), the corresponding wavelet-spectral distribution is plotted in the coordinate system $\{b, \log_2(1/a)\}$ (b is the translation parameter and a is the scaling parameter): the intensity of blackening is proportional to the squared magnitude of the function (10). The inhomogeneity of blackening of the lower, middle, and upper parts of the image in Fig. 1b shows that the initial image (Fig. 1a) contains structural elements of small, medium, and large scales, respectively. In other words, the appearance of the lower, middle, and upper parts of the waveletogram shows the presence of small-, medium-, and large-scale structures. The specific feature of the waveletogram shown in Fig. 1b is that the structural elements of the same type (light "arches" with a dark middle part) appear periodically with a certain noninteger step along the vertical line, which shows that the raster possesses self-similarity. The step size, which can be determined by measuring, for example, the vertical distances between the horizontal levels at which the tops of the "arches" are located, is related to the fractal dimension of the corresponding fractal structure. In our model example (the Cantor set), the step size is equal to $\log_2 3$.

We consider the two-dimensional images of idealized piecewise-regular structures that are the models of the images of real objects. The procedure of wavelet-spectral analysis allows one to determine the specific features of their structures.

Figure 2a shows a structure that consists of black and white squares arranged in a chessboard fashion. The linear dimensions of the squares in the right part of the structure are four times smaller that those in the left part. The one-dimensional distribution $f(t)$ is obtained by scanning along the inclined segment shown in Fig. 2a from $t = 0$ (the left end of the segment) to $t = 1$ (the right end of the segment). In the waveletogram plotted with the use of a "sombrero" wavelet (Fig. 2b), the boundaries of the horizontal bands which consist of alternating dark and light vertical columns are determined by the conditions $4 < \log_2(1/a) < 6$ and $6 < \log_2(1/a) < 8$ for the left and right parts of the image, respectively. The presence of the horizontal band (or several bands at different levels) is indicative of the periodic repetition of structural elements with a certain characteristic period (or several periods). In this case, the band in the left part of the waveletogram is two units lower than that ii the right part, which shows that the structure shown in the right part of Fig. 2a

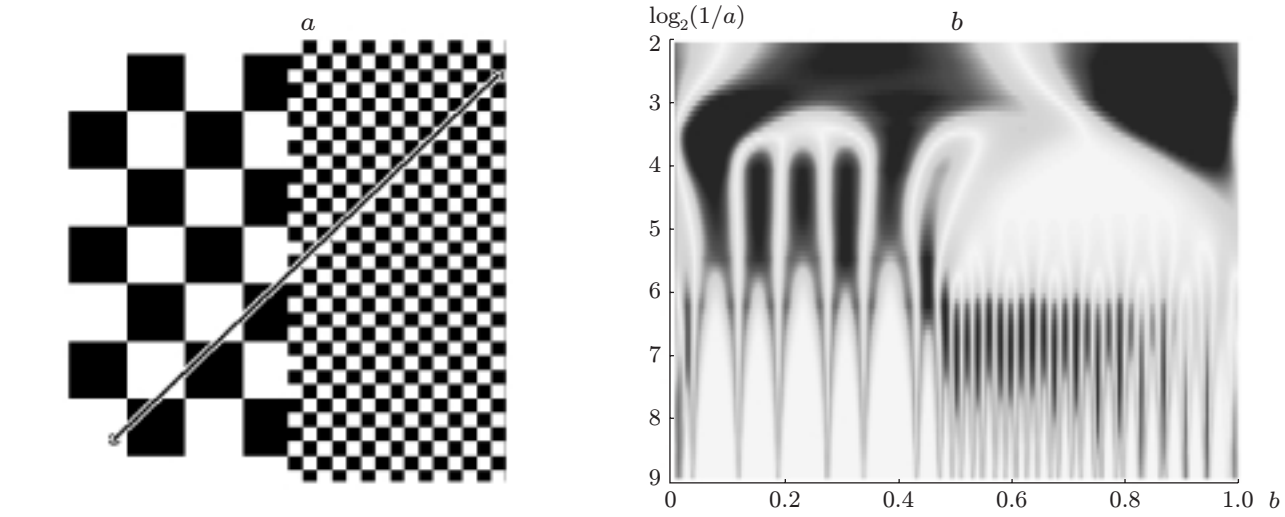

Fig. 2. Regular structure with a ratio of element sizes of 1:4 (a) and its waveletogram (b).

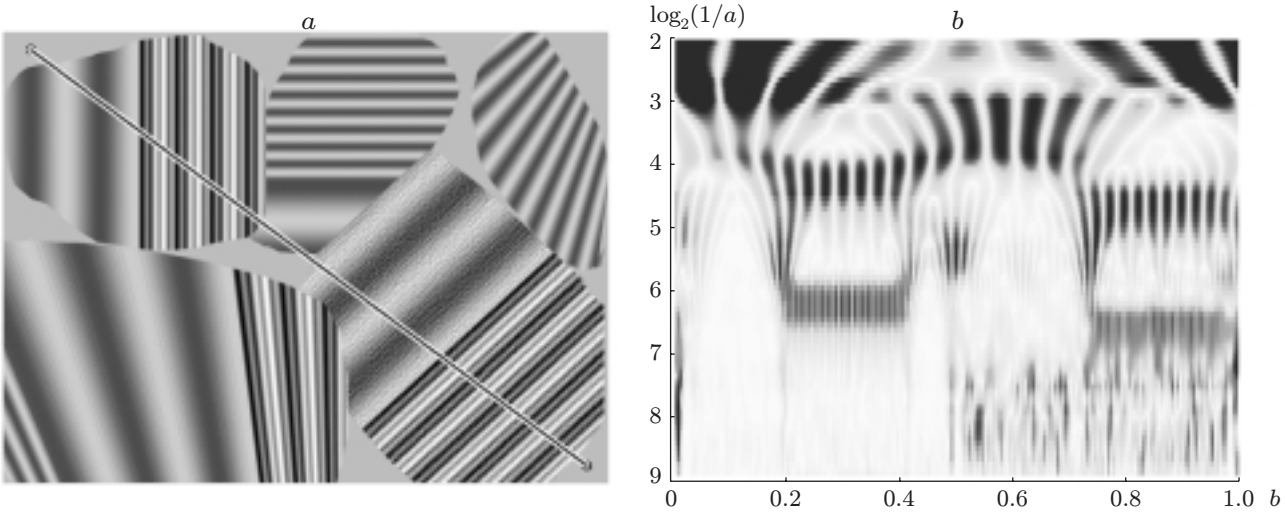

Fig. 3. Essentially two-dimensional model structure (a) and its waveletogram (b).

can be obtained from the structure shown in the left part of Fig. 2a by a proportional, fourfold contraction ($2^2 = 4$).

The essentially two-dimensional structure shown in Fig. 3a comprises a series of domains filled with model textures. Interpretation of the waveletogram plotted with the use of scanning results obtained along the inclined segment from left to right (the Morlet wavelet was used) (Fig. 3b) reveals the following specific features of the image structure:

— The structure is periodic for $0 < b < 0.19$ [horizontal band $2 < \log_2(1/a) < 3.3$] and $0.52 < b < 0.73$ [horizontal band $3 < \log_2(1/a) < 4.1$];

— The structure is doubly periodic for $0.19 < b < 0.41$ [horizontal bands $4 < \log_2(1/a) < 4.7$ and $6 < \log_2(1/a) < 6.7$; the periods differ by approximately a factor of 4] and $0.73 < b < 1$ [horizontal bands $4.4 < \log_2(1/a) < 5.3$ and $6.4 < \log_2(1/a) < 7.3$];

— In the region $0.5 < b < 1$, there is high-frequency noise (the inhomogeneity of the image in Fig. 3b for $7.5 < \log_2(1/a) < 9$).

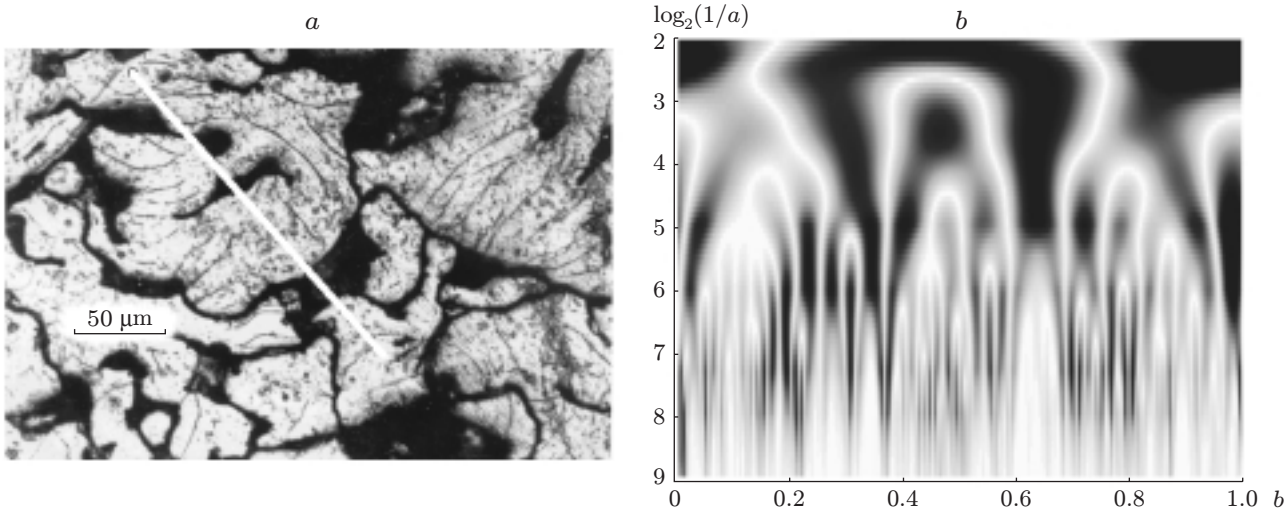

Fig. 4. The structure of titanium sponge pressed at 400 MPa (a) and its waveletogram (b).

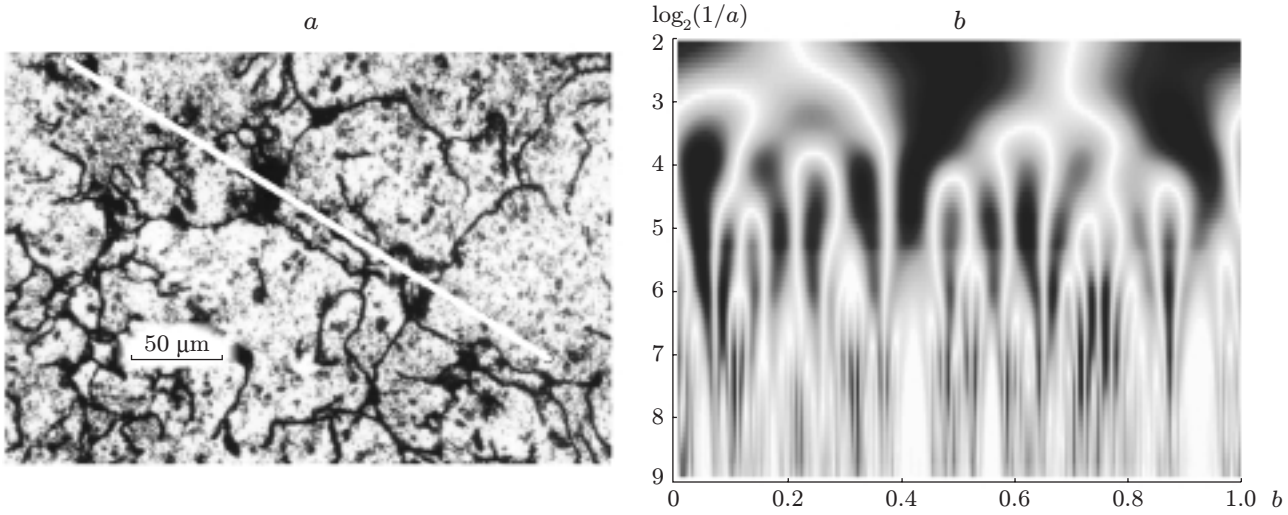

Fig. 5. The structure of titanium sponge pressed at 800 MPa (a) and its waveletogram (b).

Let us use the wavelet analysis to determine the structure of briquettes fabricated by cool compaction of titanium sponge in a closed mould at 400 (Fig. 4a) and 800 MPa (Fig. 5a). Results of mathematical and real-scale modeling and results of investigation of the structure and mechanical properties of semifinished items obtained by briquetting titanium sponge and subsequent extrusion of bars are given in [13, 14]. These investigations were performed with allowance for the fact that semifinished items and articles from technically pure titanium, whose chemical composition is identical to that of the sponge, can be obtained directly from the titanium sponge by means of the ingot-free technology, which is energy-, material-, and labor-saving.

Figures 4b and 5b show results of the wavelet transforms ("sombrero" wavelet) of the signals along the chosen directions (white line of length 200 and 290 μm in Figs. 4a and 5a, respectively). It is noteworthy that the wavelet spectrum in Fig. 4b shows that the structure of the titanium briquette is periodic with a step of 55 μm at the level of five units and the wavelet Fig. 5b shows that the structure of the titanium briquette is periodic with a step of 115 μm at the level of four units. One can infer that the more porous briquette (Fig. 4a) possesses a periodic structure at the level of five units (medium-scale level), the distance between the structural formations being of the order of 55 μm, whereas the more dense briquette (Fig. 5a) possesses

a periodic structure characterized by a step size of 115 μm at the level of four units (small-scale level). In constructing constitutive relations for structurally inhomogeneous materials (hardening curves or equations of state) at the level of mesomechanics and in determining the effective characteristics [1, 15], it is expedient to take into account the scales of structural periodic formations.

Thus, the wavelet analysis can be used to identify the structurally inhomogeneous deformable bodies. In particular, this analysis allows one to reveal whether the superficially chaotic structures possess the periodicity and determine the scale levels of representative volumes.

REFERENCES

1. I. N. Bogachev, A. A. Vainshtein, and S. D. Volkov, *Statistical Metal Science* [in Russian], Metallurgiya, Moscow (1984).
2. I. Daubechies, "The wavelets and filter banks: Theory and design," *IEEE Trans. Signal Process* **36**, No. 5, 674–693 (1989).
3. A. Grossmann and J. Morlet, "Decomposition of Hardy functions into square integrable wavelets of constant shape," *SIAM J. Math. Anal.*, **15**, 723–736 (1984).
4. N. M. Astaf'eva, "Wavelet analysis: Fundamentals of the theory and applications," *Usp. Fiz. Nauk*, **166**, No. 11, 1145–1170 (1996).
5. Y. Wu and R. Du, "Feature extraction and assessment using wavelet packets for monitoring of machining processes," *Mech. Syst. Signal Process*, **10**, No. 1, 29–53 (1996).
6. J. S. Walker, "Fourier analysis and wavelet analysis," *Notices Amer. Math. Soc.*, **44**, 658 (1997).
7. C. Bowman, T. Passot, M. Assenheimer, and A. C. Newell, "A wavelet based algorithm for pattern analysis," *Physica D*, **119**, 250–282 (1998).
8. B. Torresani, "An overwiev of wavelet analysis and time–frequency analysis (minicourse)," in: *Self-Similar Systems*, Proc. of the Int. Workshop (Dubna, Russia, July 30–Aug. 7, 1998), Dubna (1999), pp. 9–34.
9. H. Weyl, *The Theory of Groups and Quantum Mechanics* [Russian translation], Nauka, Moscow (1986).
10. J. E. Moyal, *Proc. Cambr, Phil. Soc.*, **45**, 99 (1949).
11. E. Wigner, "On the quantum corrections for thermodynamic equilibrium," *Phys. Rev.*, **40**, 749–759 (1932).
12. V. I. Tatarskii, "The Wigner representation of quantum mechanics," *Usp. Fiz. Nauk*, **139**, No. 4, 587–619 (1983).
13. A. G. Zalazinskii, V. I. Novozhonov, V. L. Kolmykov, and M. V. Sokolov, "Modeling of pressing briquettes and of extrusion of bars from titanium sponge," *Metally*, No. 6, 64–68 (1997).
14. V. I. Novozhonov, A. G. Zalazinskii, L. S. Davydova, et al., "Possibility of manufacturing bars from titanium sponge," *Tsvet. Metally*, No. 3, 91–92 (1999).
15. Yu. V. Sokolkin and A. A. Tashkinov, *Deformation and Fracture Mechanics for Structurally Inhomogeneous Bodies* [in Russian], Nauka, Moscow (1984).